The contacting and structuring of $Bi_2Sr_2Cu_1O_{6+x}$ flakes

The contacting and structuring of $Bi_2Sr_2Cu_1O_{6+x}$ flakes

Allard Nieuwesteeg

Huygens-Kamerlingh Onnes Laboratory, Leiden University
P.O. Box 9500, 2300 RA Leiden, The Netherlands

July 12, 2019

Abstract

$Bi_2Sr_2Cu_1O_{6+x}$ is a high-temperature superconductor exhibiting strange metal behaviour. A strange metal shows linear resistivity over a long range of temperatures. The strange metal behaviour can possibly be explained by the Anti-de Sitter (AdS)/Conformal Field Theory (CFT) correspondence. In order to investigate the correspondence, a method for reliably measuring the strange metal phase is required. Because measurements on macroscopic crystals deviate from the expected linear resistivity due to C-axis contribution, microscopic $Bi_2Sr_2Cu_1O_{6+x}$ flakes had to be used for the measurements. Therefore macroscopic crystals were exfoliated and the resulting flakes were contacted with electron beam lithography. Observing the strange metal regime of $Bi_2Sr_2Cu_1O_{6+x}$ under the superconducting dome furthermore requires high current densities and high magnetic fields. These prerequisites for breaking the superconducting phase were obtained by structuring the contacted flakes using a Focused Ion Beam. After successfully contacting the flakes, linear resistivity was actually observed. Calculations on a Hall-bar and a constriction then yielded values for the resistivity of $Bi_2Sr_2Cu_1O_{6+x}$ in agreement with literature. By contacting flakes showing the strange metal behaviour the first step for research into the AdS/CFT correspondence has been taken.

Contents

Chapter 1

Introduction

One of the great recent achievements of physics was the discovery of high-temperature superconductivity in 1986 in the Ba-La-Cu-O system[1] [1], having a T_c of 35 K. The discovery of BLCO spurred an enormous effort to find other cuprate materials that are high-temperature superconductors [2], resulting in the discovery of $Bi_2Sr_2Ca_1Cu_2O_{8+x}$ in 1988 [3], the first high-temperature superconductor not containing a rare earth element[2]. In the early years primarily interesting due to the superconducting properties, $Bi_2Sr_2Ca_{n-1}Cu_nO_{2n+4+x}$ has recently experienced a resurgence of attention because of the strange metal behaviour it exhibits. The strange metal behaviour, showing linear resistivity as a function of temperature, is one of the most perplexing questions of physics nowadays. A recently developed theory explains the strange metal behaviour through the AdS/CFT correspondence, a mathematical tool from string theory. Were it proven true, superficially simple linear behaviour would be explained by black holes residing in curved spacetime. The AdS/CFT correspondence also predicts hydrodynamic behaviour in $Bi_2Sr_2Ca_{n-1}Cu_nO_{2n+4+x}$, which might be proven by structuring flakes on nanometer scale. The research in this thesis focuses on contacting and structuring $Bi_2Sr_2Cu_1O_{6+x}$ flakes of a few hundred nanometer. In order to observe the strange metal phase over a long range of temperatures the form of BSCCO with a T_c as low as possible is preferred. Therefore $Bi_2Sr_2Cu_1O_{6+x}$ is chosen. Bi-2201 has a T_c of around 35 K, the lowest of the BSCCO variaties.

---

[1]For $Ba_{\frac{5}{19}}La_{\frac{90}{19}}Cu_5O_{5(3-x)}$

[2]With a T_c of 105 K

1

Chapter 2

Theory

In this chapter first the general electronic properties of BSCCO will be discussed. The behaviour of BSCCO heavily depends on the doping and the temperature. Therefore the different doping dependent phases seen in Fig. 2.1 will be discussed. Special emphasis will be placed on the strange metal phase.

2.1 BSCCO characteristics

Though BSCCO has a plethora of phases as can been seen from Fig. 2.1, in this thesis only the phases relevant to the conducted research will be discussed. The focus will therefore be on the Fermi-liquid phase, the antiferromagnetic phase, the superconducting phase and the strange metal phase. Apart from their own characteristics it is enlightening to observe their differences.

2.1.1 Physical properties

Doping

BSCCO (bismuth strontium calcium copper oxide) is a high-temperature cuprate superconductor. The general chemical formula reads $Bi_2Sr_2Ca_{n-1}Cu_nO_{2n+4+x}$, where n has a positive, integer value. As of today, BSCCO compounds for the first four n's have been synthesised. The general way to refer to a certain BSCCO compound is by writing Bi-22XY were X and Y take the value of the subscript of calcium e.g. copper. The compound used in our research is Bi-2201. Since this compound contains
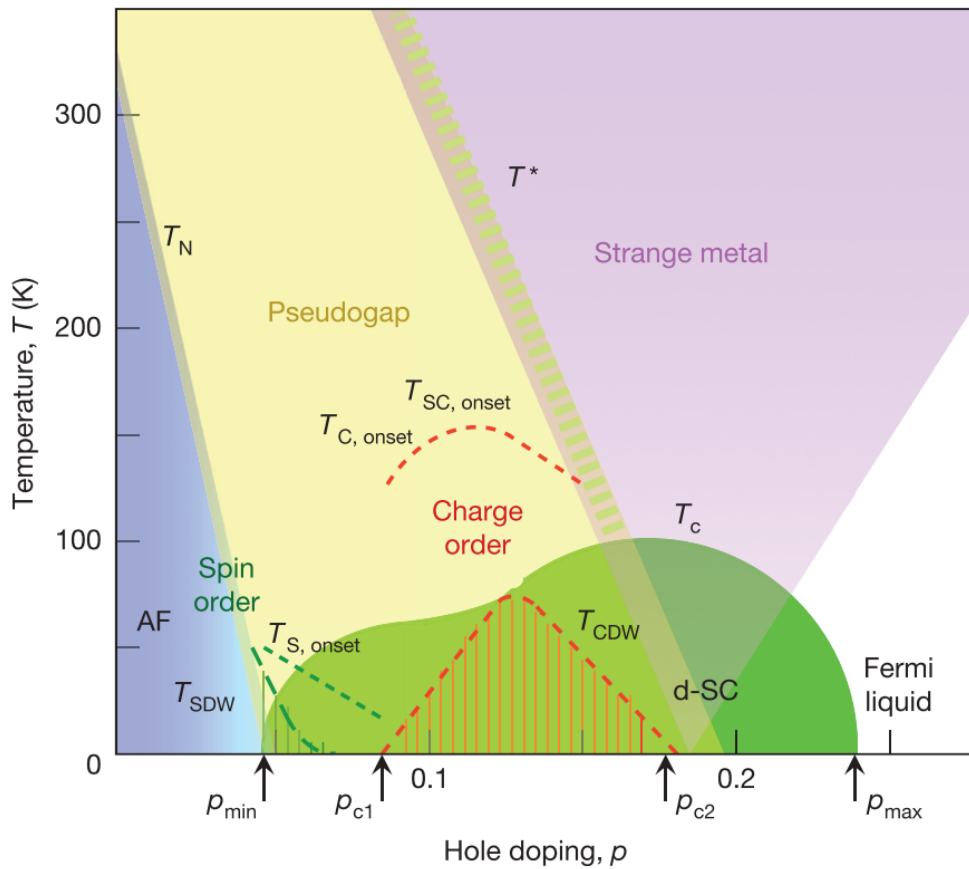
Figure 2.1: *Phase diagram of Bi-2212. The horizontal axis indicates the amount of doping in the crystal. The doping is caused by an excess of oxygen atoms. Image taken from [4]*

no calcium the C in BSCCO is dropped when writing about it specifically. Apart from the tweaking of the value n for BSCCO the oxygen content can also be changed. This is represented by the x in the compound formula. The oxygen content in BSCCO is called the doping. By doping BSCCO with oxygen atoms holes are introduced into the electronic structure. Depending on the doping BSCCO exhibits different behaviour as can be seen from the phase diagram Fig. 2.1. Different doping levels are achieved by growing an oxygen rich crystal and then annealing it in an inert environment. The amount of oxygen atoms in BSCCO that results in the highest critical temperature (T_c) is called optimal doping [5]. A crystal with fewer oxygen atoms is called underdoped, a crystal with more is called overdoped. For Bi-2201 a perfectly doped crystal results in a T_c of 33 K. The highest possible T_c is for Bi-2223 which is about 110 K. Be-
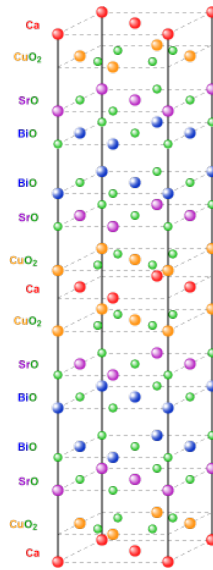
Figure 2.2: *The structure of the Bi-2212 crystal. Notice how the CuO_2 layers are seperated by insulating BiO and SrO layers. Image taken from [7]*

ing mainly interested in the strange metal phase, the samples being used are not necessarily optimally doped. Because Bi-2201 has the lowest T_c and therefore a long strange metal phase our investigation focuses on this specific form of BSCCO.

Structure

As seen from Fig. 2.2 BSCCO is a layered cake-like crystal. A crystal having a structure of two-dimensional planes bonded to each other by van der Waals forces is called a perovskite. Conducting copper-oxide planes are seperated by insulating bismuth/calcium planes. The links between the planes in the z-direction are van der Waals bonds. Since these bonds are weaker than the in-plane bonds the peeling of layers of the BSCCO can be done rather easily. It is possible to seperate the layers by pulling them apart with scotch-tape, this process is called mechanical exfoliation. Exfoliation was pioneered by Geim and Novoselov [6] on graphene. Due to the perovskite structure both ordinary conductivity and superconductivity take place mainly in the copper-oxide planes. The anisotropy of the conductivity between the out of plane C-axis and the in plane AB-axis depends on the doping and the specific BSCCO compound but can be up to a ratio of 10^4.

2.1.2 Antiferromagnetic phase

In the extreme underdoped regime BSCCO exhibits an antiferromagnetic phase Fig. 2.1. Due to a lack of hole doping BSCCO is a Mott-insulator in this state. A general Mott-insulator is monovalent and has a half filled band like ordinary metals, and therefore is supposed to be conductive. However when we imagine the crystal lattice at A1 in Fig. 2.3 this in not so evident. Notice how every electron resides at one site. Due to strong electron-electron repulsion there is a massive penalty for two electrons to be on the same lattice site, even with opposite spins. When there is this repulsion, despite the fact that the band is only half full, electrons still cannot move. The fact that electron-electron interactions are important already shows that we are dealing with a strongly interacting system. In the BSCCO case, strong electron-electron interaction is caused by the geometry of the crystal. Because the conducting copper layers are wedged between insulating buffer layers the coulomb potential is modified and electron-electron scattering is amplified [4].

Naturally the question arises how the Mott-insulator gives rise to an antiferromagnetic phase. An antiferromagnet has no net magnetization, but on a microscopic scale the material is still magnetically ordered. The coupling constant between neighbouring spins is negative and therefore spins try to allign anti-parallel. Antiferromagnetism can be observed using neutron diffraction [8]. A neutron with a fixed spin will scatter differently from the two different spin states of the material. Qualitatively the appearance of this phase can be understood by looking at the crystal lattice. Every site in the lattice contains only one electron, due to the aformentioned Mott-effect. Consider a state in which all spins point upward. We call the movement between lattice points "hopping". During hopping a fermion cannot change its spin. Hopping between lattice points in the case of all upward spins is impossible, because of the Fermi-exclusion principle shown by A2 in Fig. 2.3. If the spin of every alternating lattice point in now flipped, a state appears that allows for hopping, B1 in Fig. 2.3. Due to the strong electron-electron repulsion it is still extremely unlikely that an electron will hop. Still, merely the fact that the electron can hop hypothetically already reduces the total energy of the state. Quantummechanically alternatingly flipping the spins allows for the wave functions of the electrons to expand very slightly, and therefore reduce their energy.
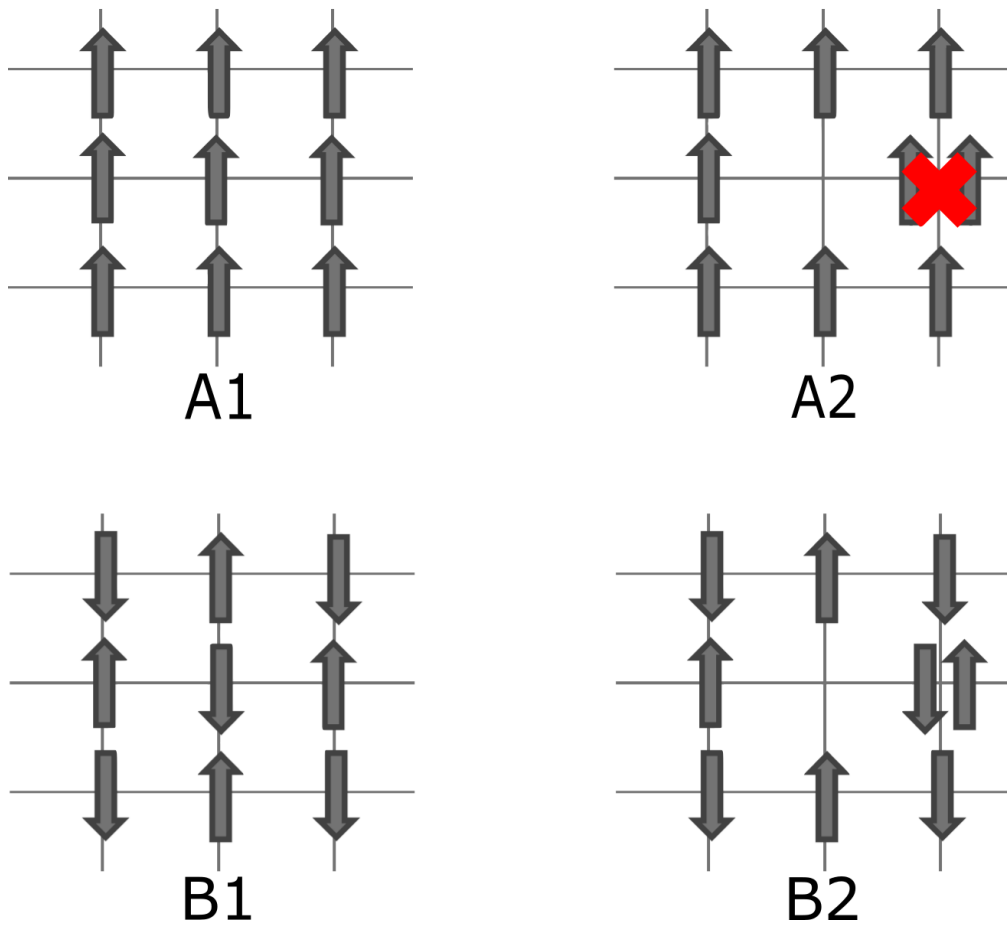
Figure 2.3: *Two spin-lattice configurations are shown. All spins in the lattice point upward in the A-configuration. In the B-configuration spins point alternatingly up and down in the lattice. In the A-configuration electrons are not allowed to hop. Adapted from [8]*

2.1.3   Fermi-liquid phase

It is now easily imaginable that adding holes to the Mott-insulator transforms it into a conductor. By creating the holes through doping the electrons actually have space to move in the lattice. Despite the increase in conductivity the electrons are still highly correlated. A highly correlated electron system can be modelled through the Fermi-liquid model. This is basically a Fermi-gass model with the non-interacting fermions substituted by interacting pseudoparticles [9]. The pseudoparticles are electrons with a modified effective mass. The change in mass results from the fact that the electron is hemmed in by other electrons. While moving to the electron crowd the electron drags some of the crowd with it. An analogy is the firing of a cannon under water. The fired cannonball carries with it the surrounding water. Apart from the change in mass the pseudoparticles also interact which each other. The Fermi-liquid phase has a quadratic resistivity at low temperatures and becomes linear at higher temperatures.

2.1.4   Strange metal phase and hydrodynamics

AdS/CFT-correspondence

The strange metal phase is the least understood phase in Fig. 2.1. The hallmark of the strange metal phase is lineair resistivity in temperature for a very broad range of temperatures. The main contrast with the Fermi-liquid phase is that at low temperatures the resistivity remains linear instead of becoming quadratic. It is remarkable that the relatively simple model of the Fermi-liquid cannot reproduce this even simpler behaviour. Though no widespread explanation exists, there are several contending theories. One of these is an explanation relying on string theory. In 1997 Maldacena [10] discovered the AdS/CFT-correspondence. AdS stands for Anti-de Sitter space, which is a space-time resulting from the Einstein-field equations with a negative cosmological constant. It is a negatively curved spacetime. A common example used to illustrate the AdS is a drawing from M.C. Escher, Fig. 2.4. CFT stands for Conformal Field Theory. A CFT is a field theory in which angles are invariant under rotation. Conformal Field Theories are used in describing several fields of physics, amongst them condensed matter physics and string theory. The correspondence means that a state in an d+2-dimensional AdS describes to same physics as a d+1-dimensional state described by a CFT [11]. This is called the holographic principle. The term refers to a hologram, which is a three-dimensional image, mapped unto a two-dimensional photographic plate.

Figure 2.4: *Shown is an Anti-de Sitter space. All triangles and squares are of the same size when taking the proper metric into account. Since an infinite amount of panes has to be traversed to reach the border, no time-like object can reach it. Image taken from [12]*

The correspondence relies on a peculiar geometrical aspect of the AdS. The AdS has an infinite surface, but a finite volume. No ordinary matter is therefore capable of travelling to the edge of spacetime, but light-like objects can. Only the light-like objects on the edge of the AdS are needed to reconstruct the bulk of it. The edge has the same dimensions as the CFT. Since the bulk of the d+2-AdS is linked to its d+1-dimensional surface, which is linked to a d+1-dimensional CFT the bulk of the AdS is linked to the CFT. Not every state in the AdS can be linked to a state in the CFT however. Only weakly perturbed states in the AdS can be mapped to strongly coupled systems described by a CFT, and vice versa.

Hydrodynamics

Recently the AdS/CFT-correspondence has been coined as a possible explanatory theory for the strange metal phase [11]. The strange metal phase is clearly a case of a highly correlated electron system. Therefore a weak perturbation is the AdS has to be found. The perturbation yielding the required correspondence is the AdS-space containing a so-called Reissner-Nordström black hole. This type of black hole is charged and therefore its electric field contributes to its mass. Despite the fact that it is called a black hole, still radiation escapes from it [13]. The black hole radiation,
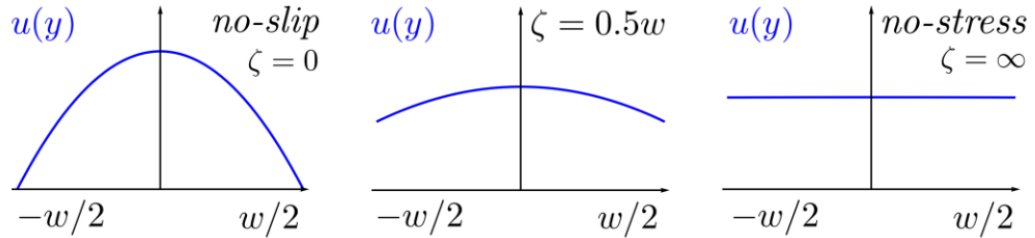
Figure 2.5: *Shown are flow profiles with different slip lengths ζ. The left picture shows a regime with no fluid moving at the boundary. The right picture shows the flow unimpeded by the boundaries. Image taken from [14]*

called Hawking radiation can be approximated as a black body spectrum with a temperature inversely related to the mass of the body. Hawking radiation causes the evaporation of every ordinary black hole given enough time. The RN-black hole is an exception to that. As the mass of the black hole decreases at a certain point only the mass attributed to electric field remains. Since it is impossible to eject the charged particles, as nothing can escape from a black hole, the black hole remains stable. By placing RN-black hole in the interior of the AdS the theory for strange metals is obtained. The correspondence predicts that strongly correlated electron system can be described by using hydrodynamics [11]. A well known fact from hydrodynamics is that the amount of transported fluid does not scale linearly with the cross-section of the channel. At the boundaries of the channel the fluid moves more slowly, and therefore the flow increases disproportianally when the cross-section is decreased. The amount by which the flow decreases is strongly dependent on the boundary conditions. For so-called no-slip boundary conditions, the fluid touching the sides of the channel does not move as can be seen from Fig. 2.5. The opposite of these, no-stress boundary conditions, generates a flow that does scale linearly with the cross-section of the channel. Since the strange metal phase can be modelled using hydrodynamics, a decrease in the current path should increase the resistivity. However, the scale at which a noticeble increase in resistivity takes place is strongly dependent on the boundary conditions, as for ordinary liquids [14]. No concensus has been reached about the boundary conditions for hydrodynamics in BSCO.

2.1.5   Superconducting regime

Two types of superconductivity

The green dome in Fig. 2.1 represents the superconducting regime. As can be seen, the superconducting regime vanishes for either heavily over-doped, or underdoped crystals. We distinguish between two types of superconductors, by the ratio of two characteristic length scales, as depicted in equation Eq.2.1.
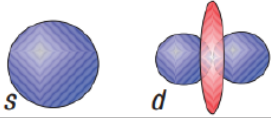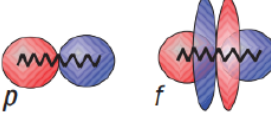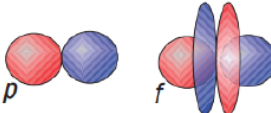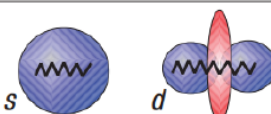
$$\kappa = \frac{\lambda}{\xi} \tag{2.1}$$

λ is the London penetration depth, characterizing how far the magnetic field penetrates into the superconductor. ξ is the coherence length, which can be interpreted as the distance between the electrons making up the Cooper-pairs. Both ξ and λ are temperature dependent through Eq.2.2 and Eq.2.3 according to Ginzburg-Landau-theory [15], which is mainly applicable around T_c.

$$\xi(T) = \frac{\xi(0)}{\sqrt{1 - T/T_c}} \tag{2.2}$$

$$\lambda(T) = \frac{\lambda(0)}{\sqrt{1 - T/T_c}} \tag{2.3}$$

Type I superconductors have $\kappa < \frac{1}{\sqrt{2}}$ and type II has $\kappa > \frac{1}{\sqrt{2}}$. BSCCO is a type II superconductor, having a coherence length of nanometers and a penetration depth of a few hundred nanometers. Though being classified as a Type II superconductor means that the mathematical tools for understanding superconductivity are applicable to BSCCO, true understanding of the high-temperature superconductivity in cuprates has proven ephemeral. An important difference between type I and type II is that a Type II superconductor can be partially penetrated by magnetic flux and still keep the superconducting properties. The local penetration of the magnetic flux is called a vortex. The onset of flux-penetration starts at a magnetic field called H_{c1}. Though the fluxs starts to penetrate the sample, the penetration flux is less than the applied field. A partially superconducting, partially normal phase is created, the so called Shubnikov phase. After reaching a field called H_{c2} the vortices merge and superconductivity is completely surpressed. A type I superconducter is either in a superconducting state, for field under H_c, or in the normal state, for fields beyond H_c. The superconducting phase can also be broken by applying a high enough current, called the critical current. The breaking of the superconducting phase is

Spin	Frequency	Momentum		
Singlet (odd)				
	Even	Even	*s*	*d*
$\uparrow\downarrow - \downarrow\uparrow$	Odd	Odd	*p*	*f*
Triplet (even)				
$\uparrow\uparrow \quad \downarrow\downarrow$	Even	Odd	*p*	*f*
$\uparrow\downarrow + \downarrow\uparrow$	Odd	Even	*s*	*d*

Figure 2.6: *Different types of states for the Cooper-pairs are given. The overal wavefunction has to be odd. The different colors of the lobes indicate opposite momenta. Taken from [16]*

then caused by the self-field, created by the supercurrent running through the wire. Both the critical current and the H_c's are inversely related to temperature in the superconductign regime. BSCCO being a type II superconductor matters. In BSCCO the H_{c1} field is rather low, but the H_{c2} field is formidable, generally increasing with several Tesla per Kelvin. At low temperatures therefore reaching the normal state by applying a magnetic field is not easily achieved. The other approach of breaking superconductivity with high critical current densities is also viable, but requires good contacts in the low temperature regime. Being very interested in the phase diagram under the superconducting dome this characteristics are tough to deal with. In order to ease the breaking of the dome samples can be structured. Since the superconducting current only flows on the edges of the current channel, by narrowing the current path the currentdensity can be increased. The increased current density generates an increased self-field which therefore breaks the superconductivity more easily.

Cooper-pair characteristics

The phenomenon of superconductivity is explained by the combination of electrons at low temperatures in so-called Cooper pairs [17]. Cooper pairs are integer spin particles and can therefore be treated as bosons. A Cooper-pairs is technically a composite boson. Since bosons are not susceptible to the Fermi-exclusion principle they can settle down collectively down in the lowest energy state. The collective settling down of the bosons is called condensation. The macroscopic wavefunction describing the bosons is called the condensate. The Cooper pair can be treated as a boson because the composite boson is a combination of two spin $\frac{1}{2}$ particles. Since the wavefunction is made up of fermions the overal wavefunction describing the Cooper-pair still has to be antisymmetric. The wavefunction is described with three variables. Spin, frequency and momentum. The spin of the composite boson in the BSCCO case is 0, called singlet state. This is an odd state. With the requirement of a total odd wavefunction either both frequency and momentum must be even, or they must both be odd. For BSCCO, both are even. While being even, still variations of both frequency and momentum are possible. Focusing on the momentum, we can imagine several states with even momentum to exist. Borrowing from atomic orbitals, different even momentum states are labeled with letters. At Fig. 2.6 different lobes are observed for different momenta. Strong evidence is arising that BSCCO is a d-wave superconductor [18]. D-wave superconductivity instead of s-wave superconductivity has major implications for the Fermi-surface of the condensate. S-pairing causes an uniform gap at the Fermi-level of roughly $K_b T$. The gap is roughly the energy it takes to break a superconducting pair. The d-pairing however causes localised gaps seen in Fig. 2.7. Instead of an uniform gap as in s-pairing, the Fermi-surface contains four nodes at $k_x = \pm k_y$. For an improved understanding of the cause of high temperature superconductivity grasping the form of the superconducting wavefunction is essential.
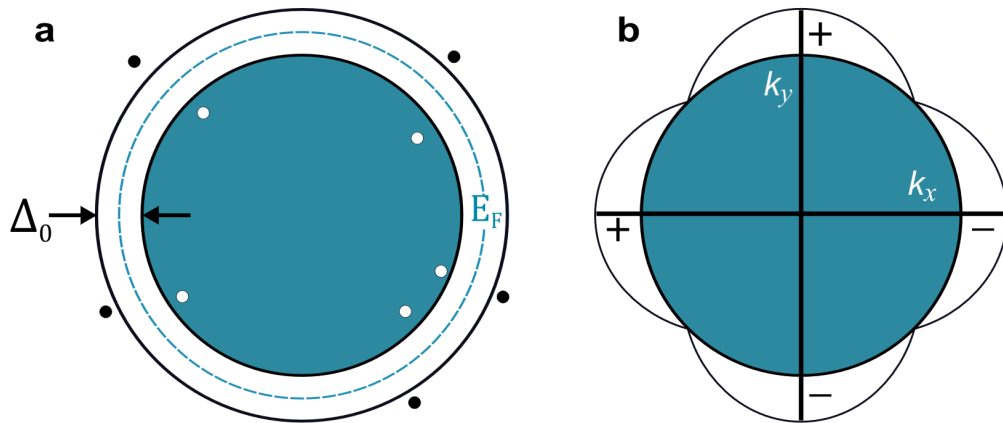
Figure 2.7: *The gap in K-space is given for two superconductors. Normally, the gap is uniform around the Fermi-surface. In the case of cuprates, at four nodes the superconducting gap is surpressed. Image taken from [19]*

3

Materials and methods

This chapter will give a description of the exfoliation and contacting of BSCO flakes followed by an explanation of the focused ion beam milling. Structuring the sample by FIB is performed for example to obtain better defined current paths and thus calculate the resistivity more accurately. In order to observe hydrodynamics performing FIB on the sample is also necessary.

3.1 BSCO-characteristics

The BSCCO we use is Bi-2201. Two batches of differently doped Bi-2201 were used. B3A1 and B3A2 with respective macroscopically determined T_c's of 23 K and 13 K. All crystals are overdoped.

3.2 Exfoliation process

Both in order to probe the hydrodynamics and the linear resistivity very thin BSCO flakes are needed. Theoretically the size of the crystal should not matter for the resistivity. In practice however non-linear behaviour is observed in a macroscopic crystal. The behaviour disappears in flakes and films. The abnormal behaviour in macroscopic crystals is probably caused by inhomogenities in the crystal. By using flakes, whiskers or films this inhomogenity is circumvented due to the small scale. In order to obtain these flakes firstly a macroscopic crystal is created. Several methods are available for crystal creation. The BSCO crystals used for our experiments are grown through the travelling-solvent floating-zone method. Some lead is added to expedite growth. After having been grown small parts of the

15

Figure 3.1: *A piece of scotch-tape with flakes. Exfoliation has been performed thrice.*

crystal are chipped of to be used as crystals for exfoliation. These chipped crystals are the size of a few millimeters.

Because BSCO is a perovskite crystal there is only weak van der Waals bonding between layers. Therefore it is possible to use the exfoliation technique invented by Geim [6] to cleave the macroscopic crystal in increasingly thinner flakes. First, a long piece of Scotch tape is put on the table, adhesive side up. Then the macroscopic crystal is picked up with a pair of tweezers and deposited at about a quarter of the length of the tape, seen from the top. Next the entire tape is folded on itself, with adhesive sides connected. Some very slight pressure is exerted with a cotton swab on the crystal between the tapes in order to improve adhesion of the crystal to the tape. Then, rather brusquely, the folded tape is pulled apart to again create one stretch. Both halves of the tape now contain crystals. A tape with crystals on it is shown in Fig. 3.1.

Carefully the macroscopic crystals are removed from the tape for reuse. There still remains sufficient crystal to continue the exfoliation. The remaining crystals wil also already be thinner than the macroscopic crystal. Continuing the procedure the tape is again folded, this time placing the BSCO residues close to each other, but not overlapping. This generally requires slight adjustment for the top piece of tape. After sticking the pieces of tape together, again a cotton swab is used to remove any air between the tape and the crystals. Again pulling of the tape energetically we end up with two crystal depositions on each side of the tape. Generally this procedure is repeated one more time, in order to obtain four depositions on each part of the tape. With any more exfolations it becomes difficult to get all the crystals on the tape on top of the substrate. An increasing

amount of tape pieces with BSCO can be created by taking a fresh piece of tape and putting it on top of a tape with four deposits. Pulling it off in the same way as done before, this creates an extra piece of usable tape.

Before transferring the tape to a Si/SiO$_2$ substrate the substrate has to be thoroughly cleaned in order to obtain maximum adhesion. The substrate is first soaked and ultrasonicated in both aceton and isopropanol for five minutes. Afterwards it is put in the PlasmaLab 90+ RIE etcher. Here the substrate is cleansed with oxygen plasma for another five minutes. The etcher removes absorbed water and other dirt from the surface. The subtrate will slowly be contaminated again after taking it out of the etcher. Therefore immediately after taking the substrates from the etcher, exfoliation is performed. Having the pieces of tape lying on the table, the just etched substrates are put on top of the BSCO crystals on the tape. Now a microscope glass is stacked on top, so that the substrate with crystal is wedged between tape and glass plate. The glass plate is added for easier handeling of the substrate and tape.

After addition of the glass plate the substrate is heated on the hotplate for 120 seconds at 100 °C. The heating procedure increases the amount of crystals sticking to the substrate. According to [20] heating of the tapes causes the gas under the flakes to escape. When cooling down the pressure under the flake is reduced and it is sucked to the surface of the substrate. Having removed the substrates from the hot plate the tape is slowly peeled off, at an angle of 45° with the substrate. In order to achieve this the substrate is pushed on the glass plate with tweezers. The almost finished substrates are submerged for 30 seconds in acetone and ultrasonicated in a short burst. This aids glue removal while minimizing the loss of and damamge to the crystals. A quick bath of isopropanol immediately follows to avoid aceton stains.

3.3   Contacting exfoliated flakes

This section will desribe the lithographic process. By refering at every step to an elucidating image, Fig. 3.2, the process will become clear.

3.3.1   Flake selection

Having deposited a large amount of crystals on the substrate, now it is necessary to identify viable crystals. A viable crystal has smooth edges and a uniformly colored surface. Each substrate is marked with a slight
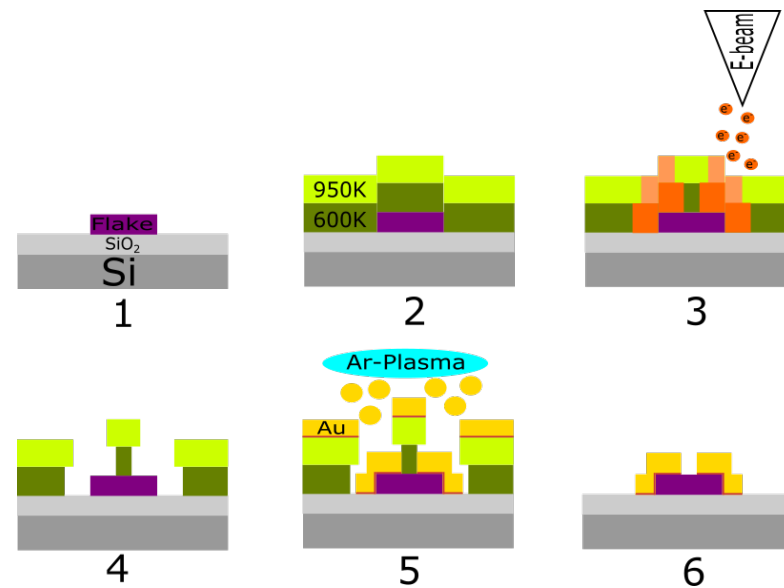
Figure 3.2: *The entire lithography-proces in one picture. 1 shows just the sample.
2 shows the application of resist, called spin-coating. 3 shows the irradiation of
the resist with the E-beam, called patterning. 4 shows the removal of destroyed
resist, called developing. 5 shows the creation of contacts through sputtering. 6
shows the sample after successfull lift-off.*

scratch in the down left corner to ensure constant orientation of the sub-
strate. The identification is done under a Nikon LV-150 optical miscro-
scope. The thickness of the BSCO-flakes is correlated with the color of
the flake. On the specific substrates used in these experiments the lighter
the shade of blue, the thinner the flake. Flakes with a brown shade are
even thinner than blue colored crystals. By performing several measure-
ments under both the profilometer and the Scanning Electron Microscope
a general feeling for the thickness of a flake can be achieved. Different
thicknesses of flakes have been contacted over the courses of the project.
Folded flakes, flakes with rough edges and flakes of more than 300 nm
were ineligible. Above 300 nm the flake would be covered with too lit-
tle resist to ensure proper lithography and hence proper lift-off. Having
found an eligible flake, both a close up picture was taken as well as an
overview picture, shown in Fig. 3.4. This overview picture must contain
at least one corner of the substrate and the flake itself. With the overview
the distance between a corner of the substrate and the flake can be mea-
sured. Later these distances can be used to move from the corner of the
substrate to the flake. Generally two flakes were selected per substrate.
This choice was a trade-off between efficiency a the quality of the crystals.
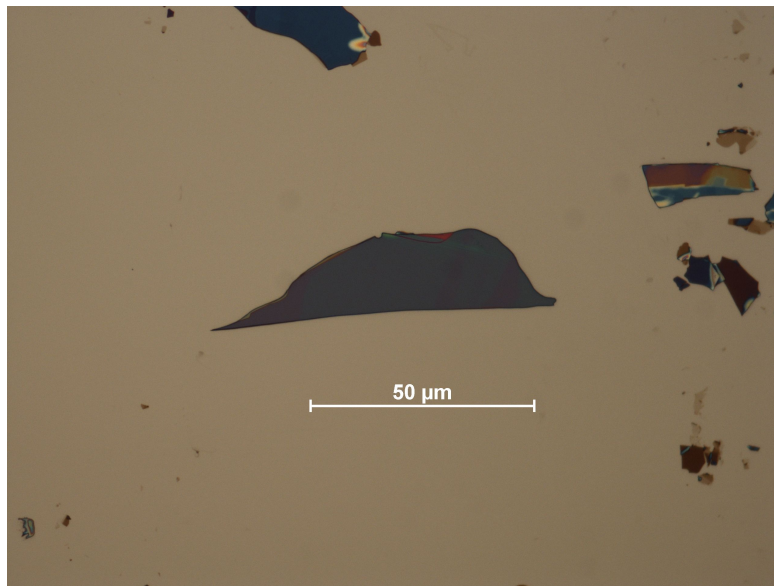
Figure 3.3: *A BSCO flake on the substrate. The color indicates a thickness of around 200 nm. The surface of the flake is also nicely smooth. The flake at the top of the image would be ineligible due to the coloring at the corner. The flakes at the right side of the picture are too small and clearly damaged.*

Contacting more flakes per substrate is more effcient than contacting the same amount of crystals on several substrates due to the time-consuming sample production. However, by having more substrates there are effectively more flakes, and thus the quality of the flakes is higher. Furthermore, especially when contacting more than three flakes per substrate the substrate becomes rather crowded and care has to be taken that contacts do not overlap. Knowing which flake to pattern on, the process can start, corresponding to 1 in Fig. 3.2.

3.3.2 Lithography

In order to write contacts to the flake Electron Beam Lithography is used (EBPG). First the sample is covered in a resist as seen in step 2 of Fig. 3.2. A resist is a solution of polymers in isopropanol. Generally the resist is polymethyl-methacrilate (PMMA). The resist is irradiated by electrons that break down the long polymers into smaller fragments. These fragments are later dissolved in a developer. A few drops of liquid resist are deposited on top of a sample. The sample is then spun around it's axis in a spincoater to achieve the required thickness. The thickness of the resulting layer of resist depends on the rotation speed and viscosity of the
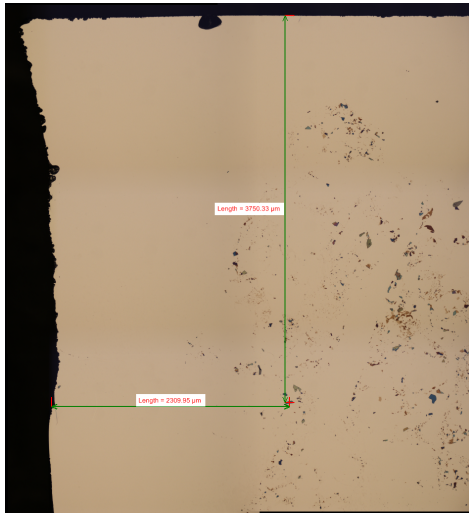
Figure 3.4: *An overview picture. The distances from the flake to the corner of the substrate are indicated. The corner of the substrate is too ill-defined to orientate from.*
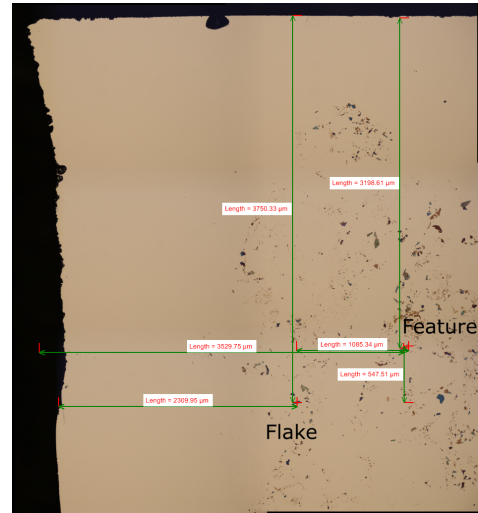
Figure 3.5: *An overview where the relative distances between a feature in the vicinity of the flake are given. First the feature is found, and then from the feature the flake is found.*

resist. After spincoating, the layer is baked at a hot plate. Multiple layers of resist can be added on top of each other. For the BSCO-samples first a layer of 600K resist with a thickness of 200 nm was applied. After spincoating the resist was baked for 60 seconds at 180 °C. Then a second layer of 950K resist with a thickness of 250 nm was applied, and baked for the same time. The K-value of a resist indicates the dose by which the resist has to be irradiated. A higher K-value means that a higher dose is necessary to destroy the resist. The 950K resist is stacked on top of the 600K in order to obtain an so called "undercut". This eases the lift-off and will be discussed in further detail later.

After placing the substrates in the EBPG (RAITH 100 EBPG) the standard focusing and writefield alignment for a field of 100 micrometer procedure is followed. This is followed by finding the corner of the flake and designating is as the origin. Before moving to the flake, first the beam is moved to a feature near the flake as can be seen from Fig. 3.5. Direct movement to the flake is too inexact. Next, with relative coordinates from the feature, the beam is moved to the flake. Then, without looking at the field of view, a high-quality picture is taken. This image has dimensions of 200μmx200μm. The picture is now appears in the patterning software. A pattern is created, where different colours mean different beam current. Large areas are written in PC1 (10 nA), smaller ones are written in PC12
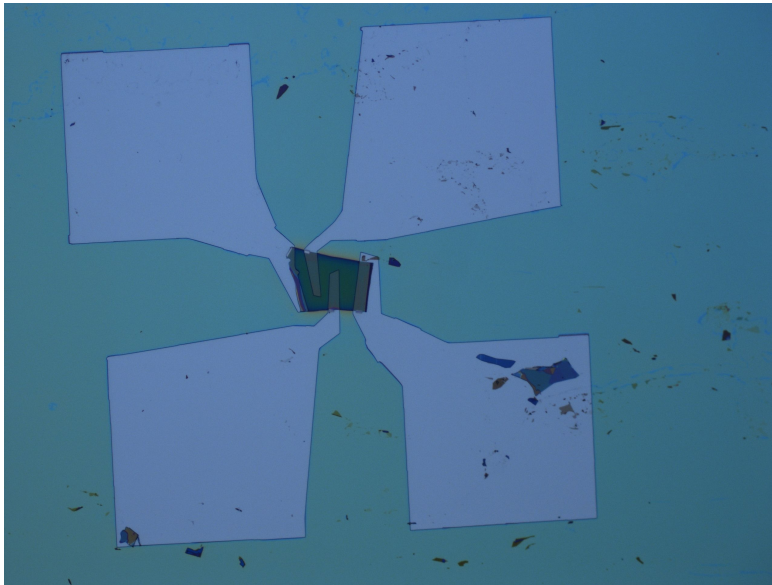
Figure 3.6: *Resist after developing*

(0.05 nA). The stepsize is one-third of the spot-size. The pattern is then written in the resist as seen from step 3 in Fig. 3.2. The E-beam can write patterns in the resist with a precision up to the tens of nanometers.

After patterning the samples are taken out and developed for 60 seconds in MIBK. The removal of irradiated resist is shown in Fig. 3.2. A few drops of water are added to improve the removal of destroyed resist. To stop the development the sample is placed in isopropanol. A example of developed resist can be seen in Fig. 3.6.

Next, metals have to be deposited on the sample in order to fabricate the contacts. For the contacting of BSCO two methods were investigated. Evaporation and sputtering.

3.3.3 Evaporation

The evaporation of silver was tried because according to [21] silver diffuses into the BSCO when baked and therefore yields very good contact resistances. Furthermore often silverepoxy is used to contact macroscopic samples.

Evaporation is a process in which a metal is heated and thereby evaporates. Due to the energy imparted by heating the evaporated particles move towards the substrate, condensating on the surface. Evaporation takes place in vacuum of around $1E^{-7}$millibar. The heating of the metal is
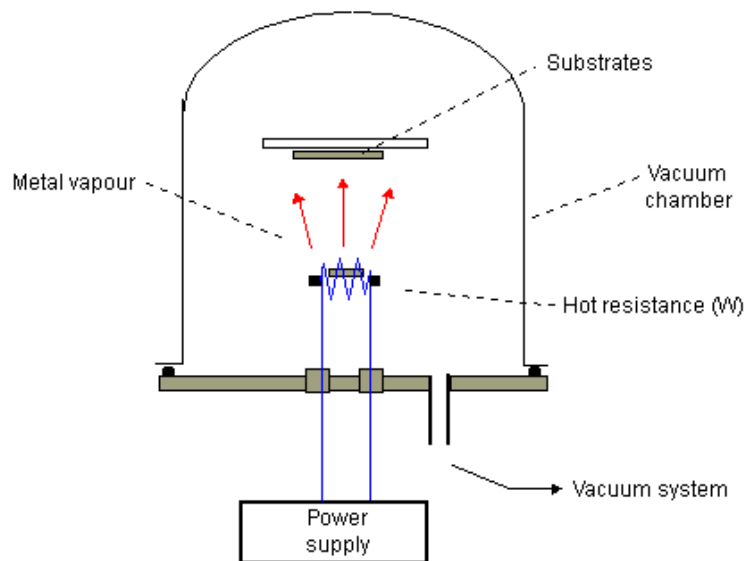
Figure 3.7: *Showing an evaporator. The metal is heated by a resistance connected to a power supply. The metal vapour created by the heating then is deposited on the sample. Image adapted from [22]*

provided by passing a high current through the holder in which the metal pellets are placed, the so-called boat. The current applied was 120 ampère. The metal can be heated beyond 1000 K. Due to the high vacuum the evaporated particles have a mean free path of several meters. Since the mean free path is bigger than the travelling distance the evaporated metal will arrive very unidirectionally. The unidirectionality is advantageous for the lift-off since it prevents the atoms from sticking to the sides of the resist. In the case of silver an easy lift-off is extra important since silver has very poor adhesion to the silicon substrate. The silver layer was varied between 100 and 200 nm and a gold layer of 30 nm was evaporated on top to protect the silver from tarnishing.

3.3.4   Sputtering

Sputtering is a process in which a plasma is ignited between the sample and the so-called sputtering target. The target, confusingly, is not the substrate but the container of the substance to be sputtered. Due to the impact of the ions particles of the target get ejected. The ejected particles scatter throught the plasma and are deposited on the substrate placed opposite to the target, shown as step 5 in Fig. 3.2. The gas used for creating the plasma is Argon, however alternatives, for example other noble gasses, are also
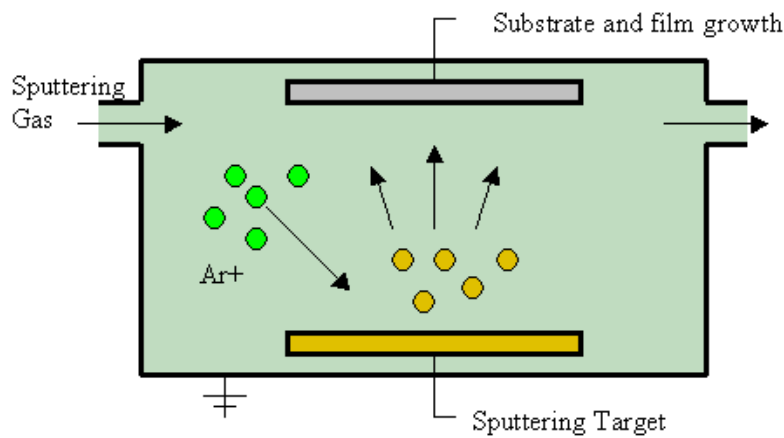
Figure 3.8: *The sputtering process is shown. A voltage difference is applied between the sample and the target causing the Argon-gas to become ionized. The positively charged ions are then attracted towards the negatively charged target. The gold ejected by their impact then covers the sample. Image taken from [23]*

possible. An electric field is applied between the target and the substrate to ionize the sputtering gas. The resulting ions are then accelerated towards the target by the voltage difference. To ensure this happens the target has a negative voltage in order to attract the positively charged gas ions. A schematic sketch of a sputtering machine can be seen in Fig. 3.8. Sputtering is not unidirectional like evaporation because the mean free path of the metal particles is much smaller. The mean-free path is smaller because the ejected gold has to move through an Argon-plasma with a pressure of around $5E^{-3}$ millibar. Thus the gold particles are continuously hit by plasma-ions and therefore change direction. Because of the multidirectionality the lift-off is more difficult. However, since it is very important to contact the flakes from the side, a multidirectional process might actually be preferred. Another disadvantage of sputtering is that the ions ejected from the target have quite a high velocity and might therefore damage the sample. The substrates were not glued to the holder so they were not thermically cooled. A rumpling of the resist was observed after sputtering, which might be caused by a lack of cooling. An example of a contacted flake can be seen at Fig. 3.9.

3.3.5 Lift-off

The sample is now covered in metal, either through sputtering or evaporation. In order the remove the metal where it is unwanted, the sam-

ple is submerged for several hours in acetone. The acetone dissolves the PMMA and thus causes the metal on top of the PMMA to come loose. The wanted metal is in direct contact with the substrate and thus adheres to it. After dissolving the resist the excess metal can be removed by spraying acetone on the submerged sample. It is very important not to let the sample out of the acetone before complete lift-off is achieved, since otherwise the remaining material will stick to the substrate and lift-off becomes nigh impossible. Generally, merely spraying with acetone is not sufficient however. To remove the stubborn pieces of metal the sample is ultrasonicated.
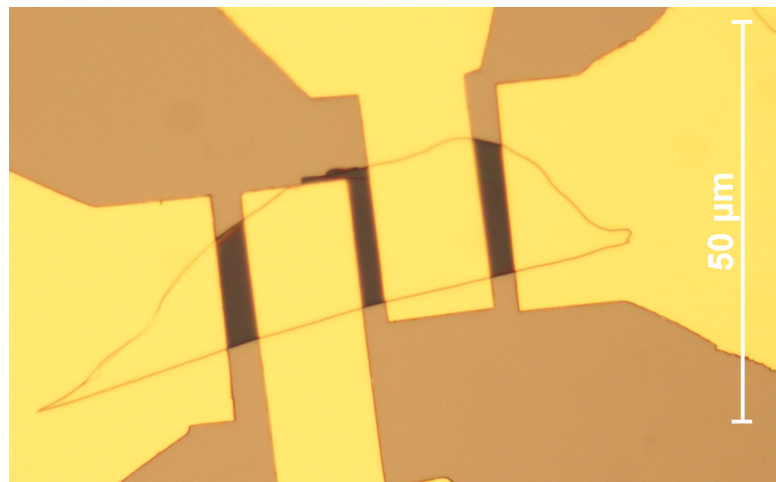

Figure 3.9: *A flake contacted with sputtered Gold contacts. The image is taken after lift-off.*

3.3.6 Focused Ion Beam

The Focused Ion Beam (FIB) is an apparatus that cuts away material and thereby allows the user to structure a sample. The cutting, called milling, is performed by a ray of ions. In this specific case the ions were Gallium. A FIB consists of a ion gun and a ordinary SEM (Scanning electron microscope). To use the FIB, first ordinary procedures for focusing the SEM are followed. The steps are extra important, since the distance between the substrate and SEM has to be know as exactly as possible. The reason for this is that both the FIB and the SEM-beam have to be focused on the same spot. If the two beams are not focused on the same spot, either the imaging of the sample is bad, or the milling process is inexact. After focusing the SEM the stage is tilted for 52°, in order for the ion gun to be perpendicular to the substrate. The rotation is performed using eucentric rotation, meaning that the SEM-beam stays focused on the same place of

the sample. Generally the FIB-ing is performed in several steps. To create the rough form of the structure high beam currents are used to speed up the milling process. As soon as the structure is approached beam currents are decreased in order to prevent damaging the nano-structure. In order to mitigate the damage done to the nano-structure by the FIB it is possible to cover the flake with a capping layer. Both flakes with and without a capping layer were structured.
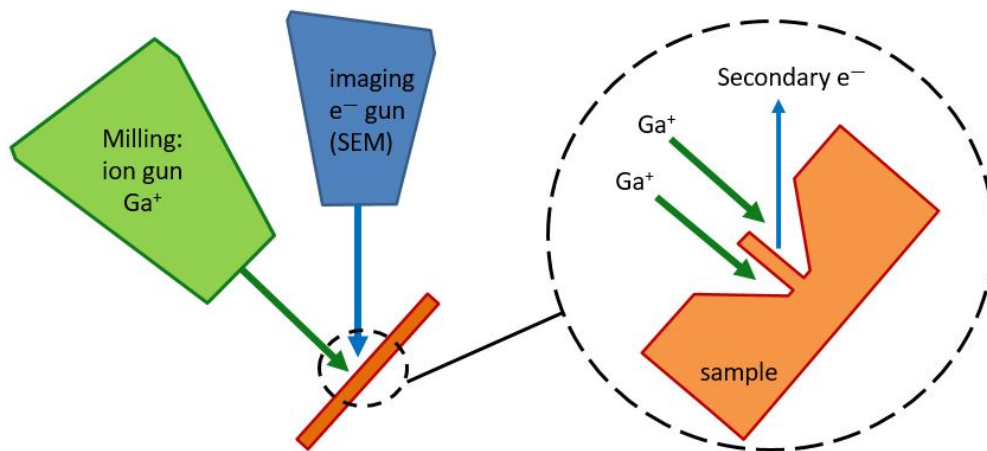
Figure 3.10: *A schematic Focused Ion Beam set up is shown. The SEM looks at the sample under an angle. Different kinds of ions can be used for the FIB. Image taken from [24]*
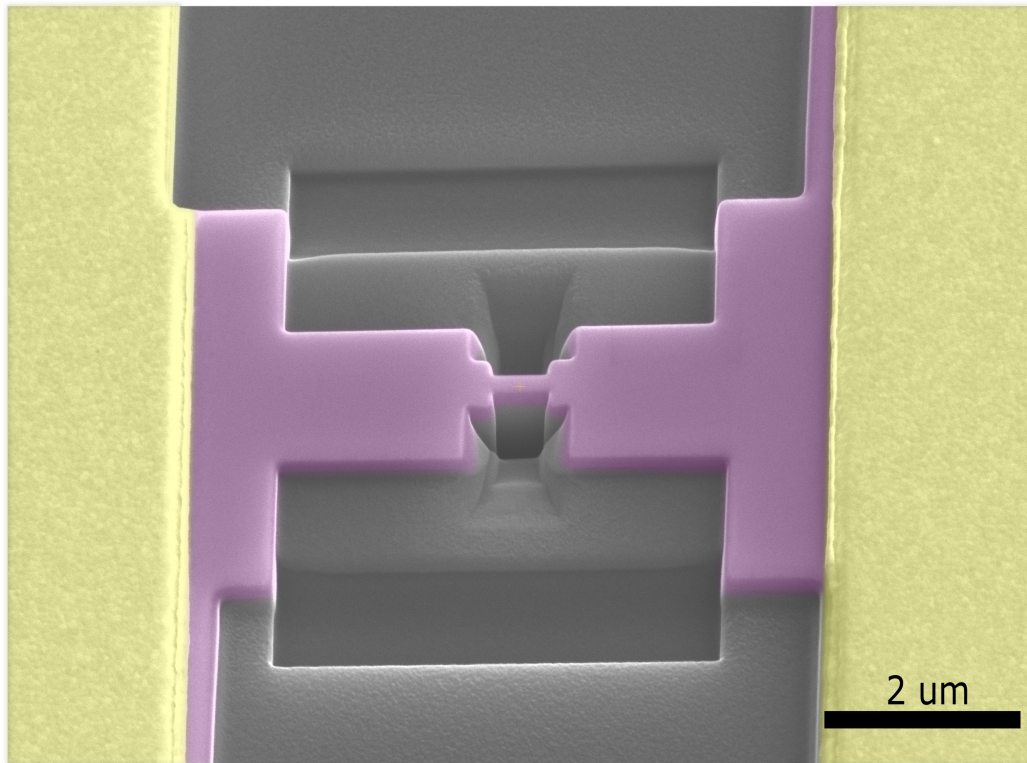
Figure 3.11: *A false colored SEM image of the FIB created nano-structure. Clearly the four steps in the process are observed, from removing big to increasingly smaller areas. The gold contacts are colored yellow. The flake is colored purple.*

Chapter 4

Results and discussion

The focus of research was two-fold. Firstly, a reliable method for contacting BSCO-flakes had to be found. Secondly measurements on the resulting contacted flakes of different thickness were to be performed, both on structured and unstructured flakes. These results will be presented in this chapter.

4.1 Contacts to BSCO flakes

4.1.1 Silver contacts

At first an attempt at contacting the flakes with evaporated silver was made. Despite the supposed ease of performing lift-off with evaporated silver still difficulties arose. When an imperfect lift-off took place, and therefore ultrasonication was needed, this almost always destroyed part of the contacts. Even using a syringe to spray acetone on the submerged sample could already cause the silver to come off.

The contact resistance of the few samples with a successfull lift-off ranged from the order of hundreds of kiloohms up to megaohms as can be seen from Fig. 4.3. To improve contact resistance the sample were baked according to the method of [21]. The contacts were annealed at 350 °C for 30 minutes with an O_2 atmosphere. The annealed samples were observed to have islands of gold on them after baking, showing in Fig. 4.1. Test were also performed on silver-contacts without the capping layer in order to ease lift-off. The results after baking these samples were detrimental. Small accumulations of material had formed, that grew whiskers when irradiated with the SEM Fig. 4.2. The substance was thought to be
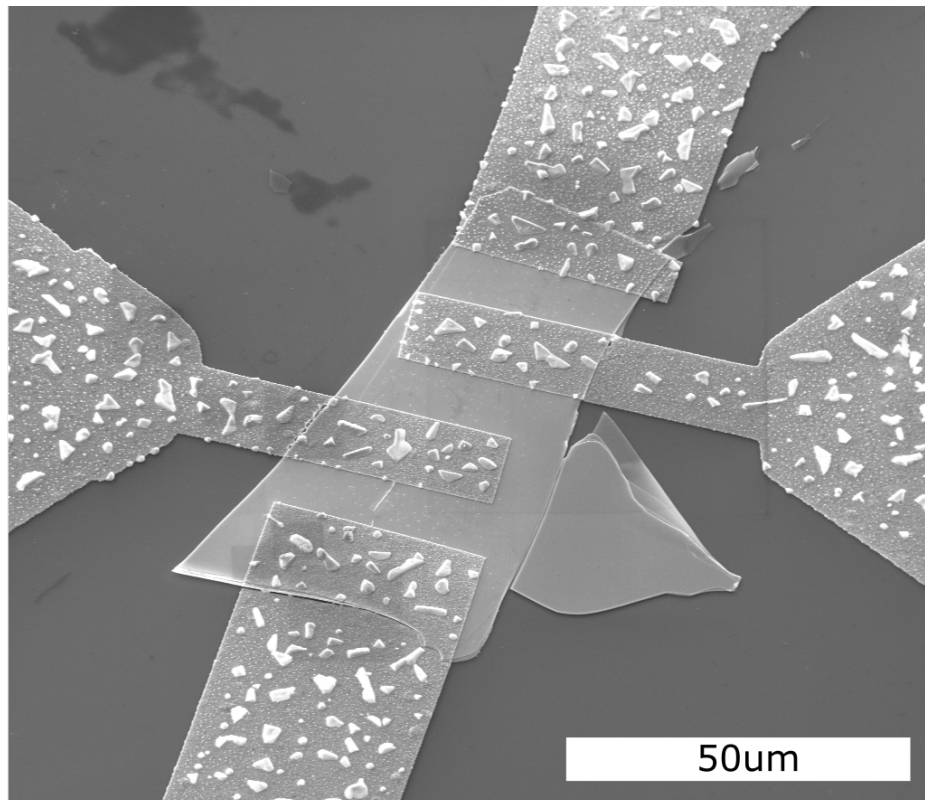
Figure 4.1: *An overview of the contacts after baking. Notice the white islands of gold that have formed on top of the silver.*

AgS_2 which returned to Ag when irradiated. Therefore either capping was truly required, or better control over the atmosphere during baking. The samples that survived the annealing process had contactresistances of tens of kiloohms Fig. 4.3. This however is still insufficient to perform reliable measurements at low temperatures. Fig. 4.3 shows the obtained resistances.

Though apparently not viable as a technique for contacting, several improvements could be made. Evaporating a thicker layer of silver might improve the contact resistance. However, in order to increase the thickness of silver, an other resist has to be used for the primary layer. The current resist allowed thicknesses of up to 200 nm. In order to improve the successful lift-off rate also two improvements could be made. Firstly a sticking layer of either titanium or chromium could be used. Secondly a very gentle lift-off, using continuously stirring magnetic pellets, could
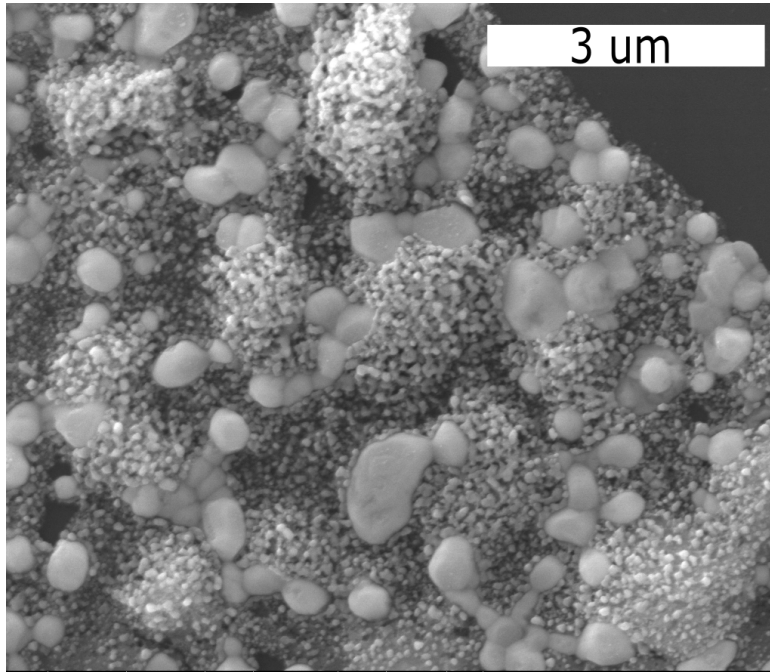
Figure 4.2: *A close-up of the contacts after baking and irradiation. The small pockmarks covering the underlying part are silver turned normal due to the SEM. Onder it lies the* SO_2*. The parts that are not pockmarked are remaining accumulations of silver.*

2-point resistance current contacts	Before baking	After baking
Sample name	MΩ	kΩ
G17F1	4.8	220
G19F1	0.87	92
G21F2	3.7	150

Figure 4.3: *Shown are the resistances of flakes contacted by Silver evaporation*

prove beneficial. If successfull lift-off rates were increased the reasearch into the annealing process and the required contact thickness would speed up greatly.

4.1.2   Gold contacts

Due to the difficulties with the silver contacts the decision was made to try sputtered gold contacts again. The first time the sputtering of 3 nm chromium as a sticking layer was tried combined with a 150 nm gold layer. Lift-off appeared to be impressively more easy when using the sputtering system. Due to the chromium sticking layer samples can be ultrasonicated which facilitates the removal of the unwanted gold. Only very rarely contacts on top of the flake come off. Whenever contacts come of it is on thick crystals. The sputtering approach yielded resistances on the order of tens of kiloohms. These values were on equal footing or even better than the values achieved with silver. Since sputtering was regarded as an improvement over evaporation, the amount of gold deposited was increased to 200 nm. This consistently yielded contact-resistances of a few hundred ohm. The tremendous improvement in resistance probably has to do with improved contacting from that side of the crystal. Due the fact that sputtering is multi-directional the side-surfaces of the flakes, which van have overhanging parts, can be completely covered Fig. 4.5. Whilst being a multidirectional process, there is still less gold deposited on the side of the flake than on top of it. Therefore it is advisable to make the contact thickness identical to the thickness of the flake.

2-point resistance current contacts	300 K	12 K
Sample name	Ω	kΩ
H2F1	2.5E+03	-
H2F2	1E+04	-
H14F1	250	16.7
H14F2	114	5.10
H15F1	141	12.8
H15F2 (Hall)	70	8.38
H16F1 (Hall)	122	2.68
H17F1	886	92.6

Figure 4.4: *Shown are the resistances of several flakes contacted by gold sputtering. The first two flakes were sputtered with 150 nm gold. The rest of the flakes was contacted with 200 nm contacts.*
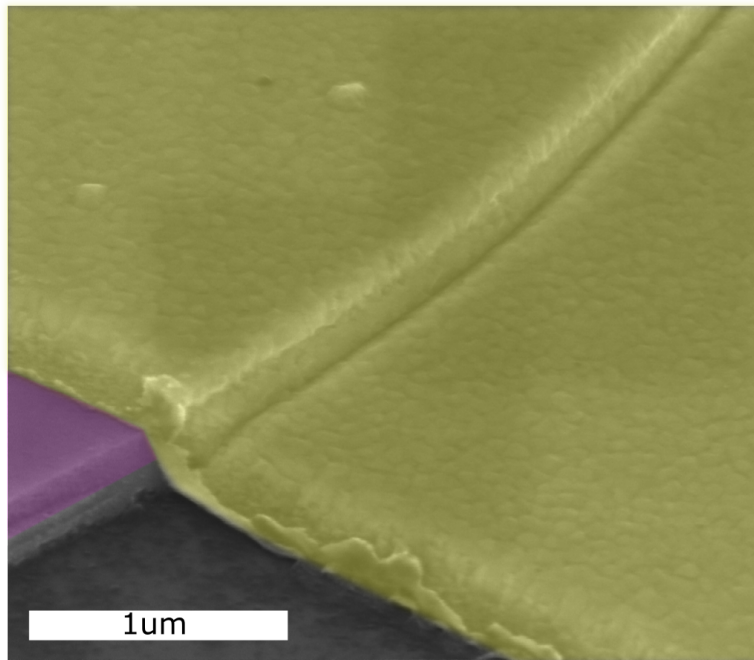
Figure 4.5: *A sputtered gold contact is shown. Notice the trench at the side of the flake where less gold is deposited. Covering the trench with evaporation would have been even more difficult.*

4.2 Measurements

After the achievement of contacting the flakes two remaining goals were set. Firstly, checking whether the flakes became truly superconducting and secondly trying to calculate the resistivity. All measurements were done in 4-probe configuration.

4.2.1 Linear resistance

Obtaining several RT-measurements showing signs of superconductivity proved possible. As Fig. 4.6 shows multiple flakes show the same linear behaviour, albeit with slightly different 4-point resistances. These differences can be explained by different contact sizes and different distances between the contacts. Especially puzzling is the difference between the critical temperatures of the flakes. All flakes shown are derived from the same crystal batch with a reported bulk T_c of 13 K. Although the differences are not huge, it is remarkable that all T_c's lie above the expected
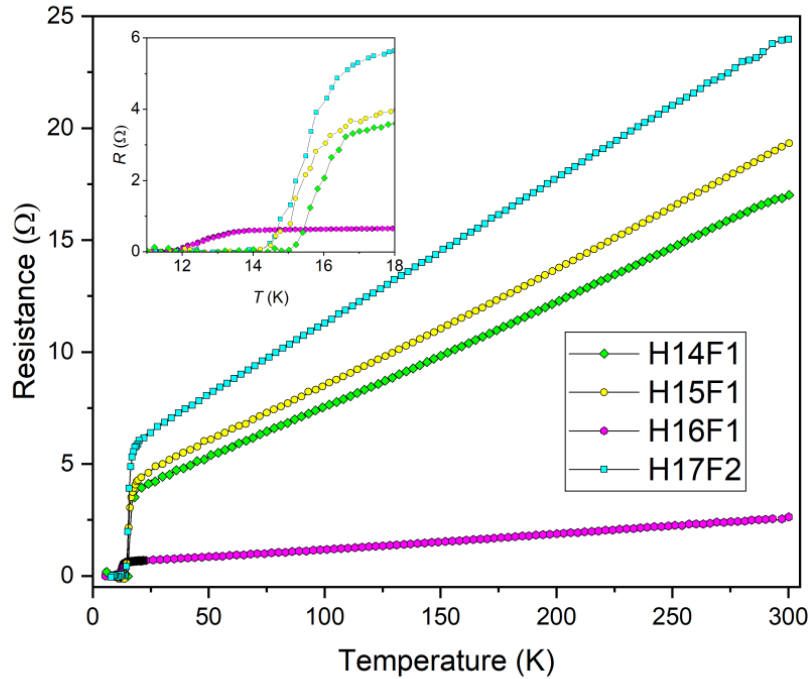
Figure 4.6: *Shown are the RT's of several flakes with a supposed T_c of 13 K. Notice the linearity of all curves, as well as the difference in T_c's.*

T_c. There are several possible solutions for this conondrum. Firstly, the microscopic crystal from which the flakes are derived could be inhomogenous. In the macroscopic crystals often there is seen a upturn in the RT just before the onset of the superconducting phase. The upturn implicates C-axis contribution to the resistivity. On a smaller scale these inhomogenities might still exist and cause differences in T_c. The T_c would than however be expected to vary around 13 K, not consistently lie above it. Secondly, the change in T_c might be caused by a loss of oxygen. The loss might both be due to ambient conditions or due to the lithography proces. Since literature [25] shows oxygen loss to be negligible on the timescale of weeks this is unlikely. Furthermore, a constriction was measured for several times over the span of a few weeks and its T_c did not change appreciably. For a nano-structure the diffusion would be most rapid since the exchange surface is huge, so no change in T_c probably means that ambient diffusion is irrelevant. Secondly the possibility exists that the heating during the sputtering and baking of the resist causes oxygen to diffuse out.

All observed values of the T_c lie above the expected T_c of 13 K. Since all crystals are overdoped the behaviour observed could actually correspond to oxygen loss. Reduces oxygen content in overdoped samples heightens the T_c. This explanantion is not completely satisfactory either since all flakes were contacted in practically the same way. Difference in exchange surface between the crystals might possibly explain the difference in T_c. A last important remark is that differences in T_c were even observed for flakes contacted in the same proces. The flakes H14F1 seen in Fig. 4.6 and Fig. 4.14, H15F1 seen in Fig. 4.6 and H15F2 seen in Fig. 4.14 were all contacted in one session. They still show appreciably different T_c's.

4.2.2 The 23K flake

One flake of the batch with a T_c of 23 Kelvin was contacted too. Though the flake does not show superconducting behaviour, the linear regime is still present. The fact that the resistance is linear suggests however that the contacting method is viable for flakes with different doping levels.
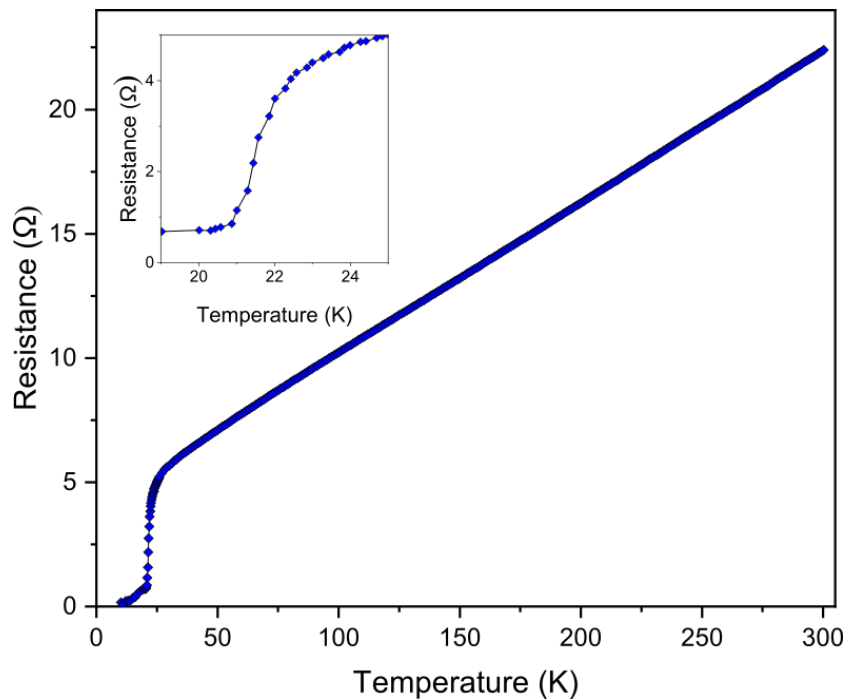

Figure 4.7: *Shown is the RT of a flake with a T_c of 23 K. The flake does not go completely superconducting but does show linear behaviour. The onset of presumed superconductivity is around T_c.*

### 4.2.3   Structured samples

The effects of structuring

In order to obtain a proper idea of the resistivity of BSCO two flakes were structured. Unsurprisingly the resistance has increased in the structured sample, as can be seen in Fig. 4.8.
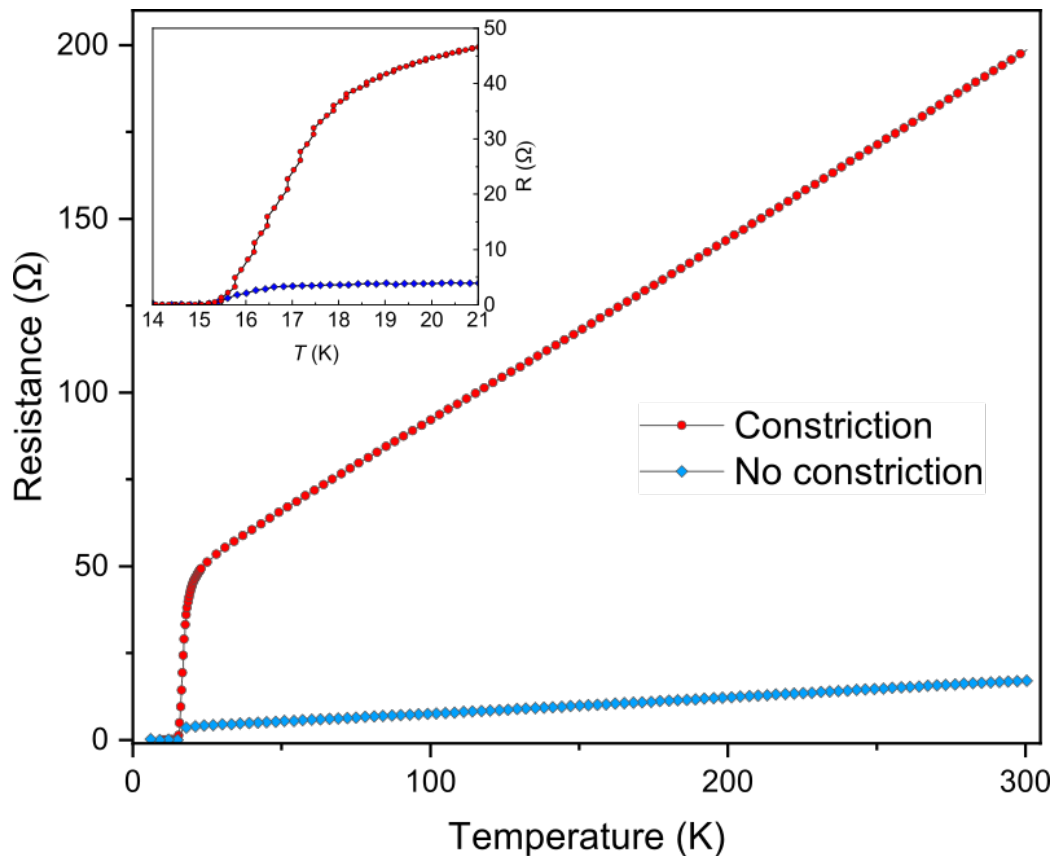
Figure 4.8: *Shown are the RT's of both the structured and unstructured flake. As expected, the resistance increases when structuring the flake and thereby reducing the current path.*

The linearity is still maintained. To observe the true effect of structuring on the flake the resistance is normalised. As can be seen from Fig. 4.9, there are two main changes. Firstly, the linearity of the graph is increased even further. The increase in linearity is caused by a better defined current path. Secondly, a slight change in the T_c is observed.
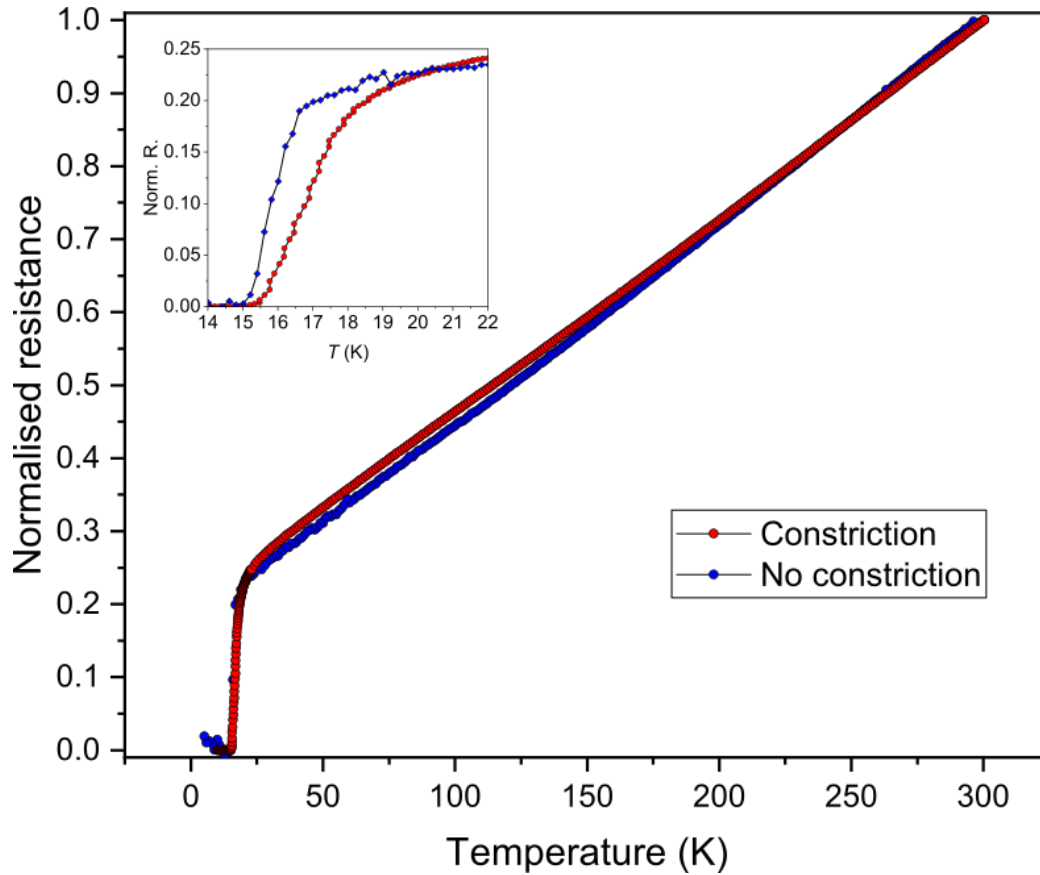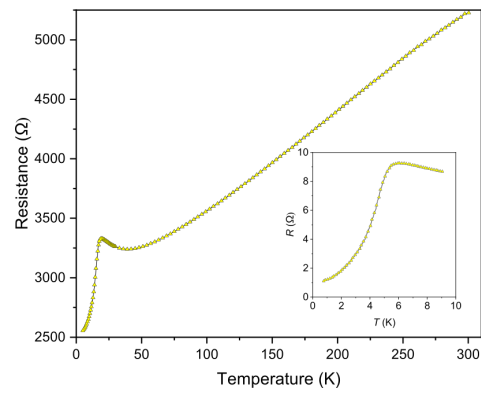
Figure 4.9: *Shown are the normalised RT's of the structured and unstructured flake. A slight deviation in T_c is observed.*

This result shows that the structured flake still generally maintains the characteristics of the unstructured flake. In order to maintain the characteristics of the flake after structuring is it however necessary to cap the flake with an additional layer of SiO_2. The flake in Fig. 4.6 was capped. Another sample that was not capped lost all properties of the microscopic flake. The differences between the unstructured Fig. 4.10 and the structured flake Fig. 4.11 are stark. First ofcourse there is the upturn between 23 and 30 Kelvin. Furthermore the resistance has increased massively. A change is resistance is expected, but not of this magnitude. Comparing the increase to Fig. 4.8 it is observed that the difference is a factor 200, instead of 10. When normalising the RT's Fig. 4.12 the disproportionallity is proven. Even the slopes of the RT's are different. The final important aspect is that the structured flake does not become superconducting.
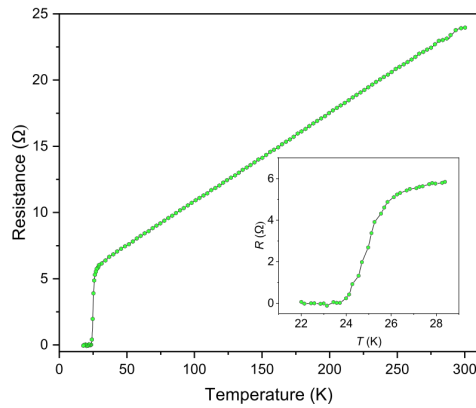
Figure 4.10: *Shown is the RT of the unstructured and uncapped flake. Macroscopic measurements yield a T_c of 13 K in constrast with the 25 K here observed.*

Figure 4.11: *Shown is the RT of the structured flake without capping. Notice the massive increase in resistance and the lack of a superconducting transition.*
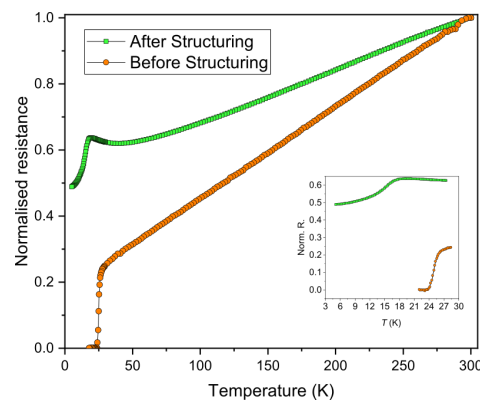

Figure 4.12: *Shown are the normalised RT's of the structured and unstructured flake. Notice the difference in slopes of the curves, especially as compared to Fig. 4.9.*

Resistivity

In total two flakes were properly structured. One flake was structured into a constriction and one into a Hall-bar. In order to calculate the resistivity of BSCO Eq.4.1 is used, where L_x is taken to be the direction of the current. The dimensions of the constriction are obtained from the SEM-images of the structures e.g. Fig. 4.13 and Fig. 4.14.

$$\rho_0 = \frac{R L_y L_z}{L_x} \tag{4.1}$$
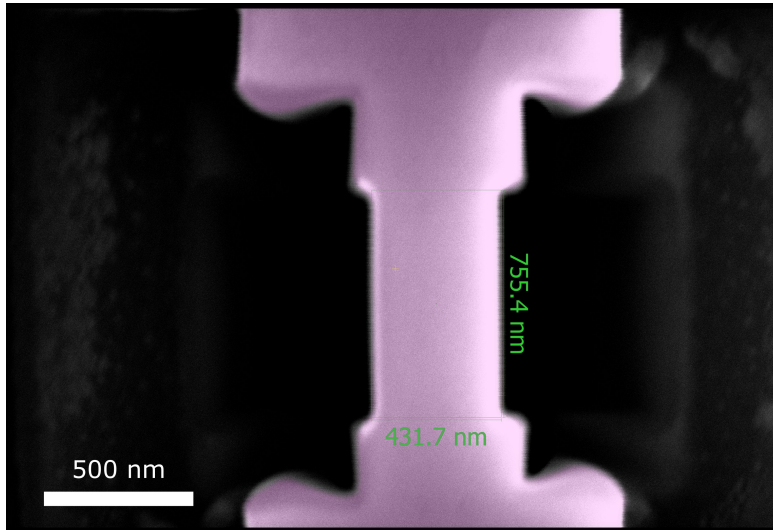
Figure 4.13: *Shown are the dimensions of the constriction. The height was determined from another SEM-image.*
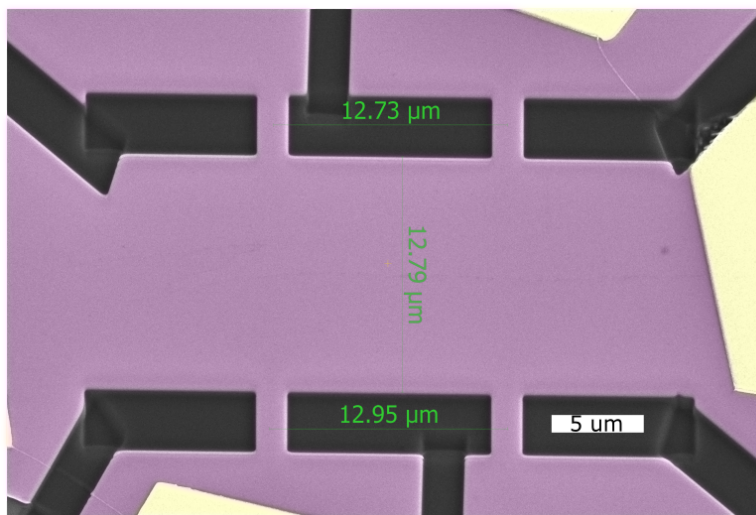

Figure 4.14: *Shown are the dimensions of the structured Hall-bar. The thickness was obtained from another SEM-image.*

For the Hall-bar Eq.4.1 readily works. Applying the formula to the constriction is slightly more difficult. As can be seen from Fig. 3.11 the

resistance measured is not only over the constriction, but also over the neighbouring parts. Effectively the resistance is measured over several serialised resistors. Incorporating this fact into Eq.4.1 results in Eq.4.2 with M the amount of serialised resistors and n the dimensions of each resistor.

$$\rho_0 = \frac{RL_z}{\sum\limits_{n}^{M} \frac{L_{xn}}{L_{yn}}} \tag{4.2}$$

Which ofcourse reduces to Eq.4.1 in the case of M = 1. Since the terms in the summation are all dimensionless they can be easily obtained from Fig. 3.11.
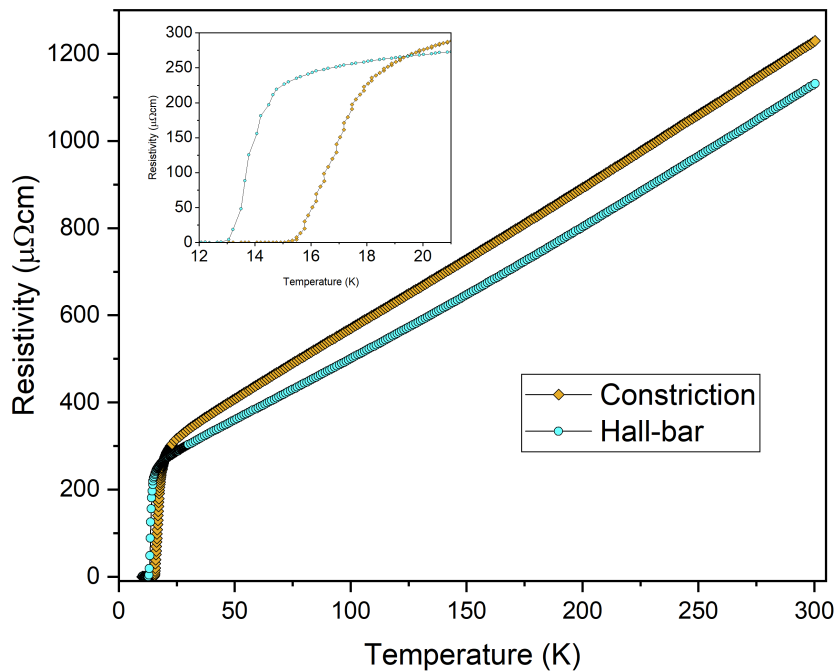
Figure 4.15: *Resistivity plot for the Hall-bar and constriction. The Hall-bar is 250 nm thick and the constriction 200 nm. The constriction is modelled as a serialized resistor.*

As can been seen from Fig. 4.15 the values of the structures are quite in agreement with each other. Though the literature [26] [27] [28] values radically differ depending on the choice and doping of the BSCCO in question, they roughly seem to correspond to the obtained values.

Chapter 5

Conclusion and outlook

The main goal of the project, obtaining good electrical contacts to BSCO-flakes has been achieved. With contact-resistances of a few hundred ohm at 300 Kelvin and several kiloohm at 12 Kelvin measurements of flakes till very low temperatures are now possible. Even below the T_c of Bi-2201 measurements can safely be done with tens of microamps. Though the favourable contacting method is gold sputtering, further research in silver evaporation might also yield good contacts. Especially when methods to improve lift-off were to be found. A capping layer on the silver contacs will be necessary to protect the silver from turning into AgS_2. The disadvantage of evaporation over sputtering will remain however due to the difficulty of contacting the sides of flakes with an unidirectional process.

The use of Bi-2201 flakes as a way to better observe the strange metal phase has also been investigated. Every properly contacted flake of sufficient thickness showed linearity untill T_c. The contacts were made on crystals for two different T_c's. Though the flake of the 23 K batch did not go superconducting, the linear regime still showed. This in contrast to macroscopically contacted flakes that often show upturns close to T_c or behave non-linear in the strange metal regime. In order to observe the strange metal phase flakes are preferred compared to macroscopic crystal. However, measurements on flakes in order to obtain the T_c and therefore the doping of a macroscopic crystal are not fully reliable or indicate inhomogenities in the macroscopic crystal. On crystals with an expected T_c of 13 K values between 13 K and 16 K were measured. It was observed that the changed T_c's are always higher than the expected T_c. Further thought has to be put into why the T_c changes due to the contacting process. The most likely candidate is the heating of flakes. The heating might be mitigated by baking the resist at lower temperatures and cooling the samples

39

while sputtering.

After having obtained exquisitely contacted flakes and observing the expected RT's an attempt was made to calculate the resistivity of Bi-2201. With the use of FIB three flakes were structured. The uncapped flake clearly showed the necessity for capping, whilst the other two maintained the microscopic characteristics. A slight change in T_c was observed. When calculating the resistivity of the flakes it was found that the values were both in correspondence with each other and rougly corresponding to literature. Since using FIB does not change the relevant characteristics of Bi-2201 in the future FIB can be used on even thinner crystals. When thin crystals can be prevented from deteriorating this would perhaps allow for the verification of hydrodynamics in strange metals. If the hydrodynamics would be verified, this would be additional proof for the AdS/CFT correspondence and its applicability to the strange metal phase.

Acknowledgements

First and foremost I want to thank Remko Fermin. Even when planning became chaotic or results were discouraging he always remained patient and optimistic, leading onward on the one path of science. Secondly I want to thank prof. dr. Jan Aarts and the entire MSM group for always providing critical but constructive feedback and support. A special thanks goes out to the technicians Douwe and Thomas who were always happy to explain the machinery to me. Thirdly I would like to thank the group from dr. E. van Heumen for providing the BSCO-crystals. Finally I would like to thank my roommates, Elgar, Tycho, Bart and Amber for the fun and inspiring discussions we had about physics and every other conceivable subject.

Bibliography

[1] J. G. Bednorz and K. A. Müller, *Possible High* T_c *Superconductivity in the Ba-La-Cu-O system*, Z. Phys. B **64**, 189 (1986).

[2] M. K. Wu, J. R. Ashburn, C. J. Torng, P. H. Hor, R. L. Meng, L. Gao, Z. J. Huang, Y. Q. Wang, and C. W. Chu, *Superconductivity at 93 K in a new mixed-phase Y-Ba-Cu-O compound system at ambient pressure*, Phys. Rev. Lett. **58**, 908 (1987).

[3] H. Maeda, Y. Tanaka, M. Fukutomi, and T. Asano, *A New High-TcOxide Superconductor without a Rare Earth Element*, Japanese Journal of Applied Physics **27**, L209 (1988).

[4] B. Keimer, S. A. Kivelson, M. R. Norman, S. Uchida, and J. Zaanen, *From quantum matter to high-temperature superconductivity in copper oxides*, Nature **518**, 179 (2015).

[5] M. R. Presland, J. L. Tallon, R. G. Buckley, R. S. Liu, and N. E. Flower, *General trends in oxygen stoichiometry effects on*, Physica C **176**, 95 (1991).

[6] K. S. Novoselov, A. K. Geim, S. V. Morozov, D. Jiang, Y. Zhang, S. V. Dubonos, I. V. Grigorieva, and A. A. Firsov, *Electric Field Effect in Atomically Thin Carbon Films*, Science **306**, 666 (2004).

[7] *BSCCO structure*, `https://en.wikipedia.org/wiki/Bismuth_strontium_calcium_copper_oxide#/media/File:Bi2212_Unit_Cell.png`, Accessed: 2019-06-25.

[8] S. H. Simon, *The Oxford Solid State Basics*, Oxford University Press, 2013.

[9] G. Baym and C. Pethick, *Landau Fermi-liquid theory*, John Wiley and Sons, Inc, 1991.

[10] J. Maldacena, *The large N Limit of superconformal field theories and supergravity*, Advances in Theoretical and Mathematical Physics **2**, 231 (1998).

[11] J. Zaanen, Y. Liu, Y.-W. Sun, and K. Schalm, *Holographic Duality in Condensed Matter Physics*, Cambridge University Press, Cambridge, 2015.

[12] *Circle limit III*, https://www.mcescher.com/gallery/recognition-success/circle-limit-iii/, Accessed: 2019-06-17.

[13] S. W. Hawking, *Particle creation by black holes*, Communications in Mathematical Physics **43**, 199 (1975).

[14] E. I. Kiselev and J. Schmalian, *Boundary conditions of viscous electron flow*, Physical Review B **99**, 1 (2019).

[15] M. Tinkham, *An introduction to Superconductivity*, Dover publications, 1996.

[16] M. Eschrig and T. Löfwander, *Triplet supercurrents in clean and disordered half-metallic ferromagnets*, Nature Physics **5**, 138 (2008).

[17] J. Bardeen, L. N. Cooper, and J. R. Schrieffer, *Microscopic Theory of Superconductivity*, Phys. Rev. **106**, 162 (1957).

[18] C. C. Tsuei and J. R. Kirtley, *Pairing symmetry in cuprate superconductors*, Rev. Mod. Phys. **72**, 969 (2000).

[19] K. Lahabi, *Spin-triplet supercurrents of odd and even parity in nanostructured devices*, PhD thesis Leiden university, 2018.

[20] Y. Huang, E. Sutter, N. N. Shi, J. Zheng, T. Yang, D. Englund, H. J. Gao, and P. Sutter, *Reliable Exfoliation of Large-Area High-Quality Flakes of Graphene and Other Two-Dimensional Materials*, ACS Nano **9**, 10612 (2015).

[21] S. Suzuki, H. Taniguchi, T. Kawakami, M. Cosset-cheneau, T. Arakawa, S. Miyasaka, S. Tajima, Y. Niimi, and K. Kobayashi, *Electrical contacts to thin layers of $Bi_2Sr_2CaCu_2O_{8+\delta}$*, **053201**, 11 (2018).

[22] *Evaporator Image*, `https://www.researchgate.net/figure/a-Thermal-evaporation-coating-unit-b-schematic-of-resistive-coating_fig2_323661379`, Accessed: 2019-06-17.

[23] *Sputtering Image*, `https://en.wikipedia.org/wiki/Sputter_deposition#/media/File:Sputtering2.gif`, Accessed: 2019-06-15.

[24] *FIB Image*, `http://m6fossils.univ-lille.fr/fr/techniques/focused-ion-beam`, Accessed: 2019-06-18.

[25] C. Paolini, P. Benzi, P. Volpe, C. Manfredotti, P. Olivero, M. Truccato, G. Rinaudo, and A. Agostino, *Growth, contacting and ageing of superconducting Bi-2212 whiskers*, Superconductor Science and Technology **15**, 1304 (2002).

[26] S. Martin, A. T. Fiory, R. M. Fleming, L. F. Schneemeyer, and J. V. Waszczak, *Temperature dependence of the resistivity tensor in superconducting $Bi_2Sr_{2.2}Ca_{0.8}Cu_2O_8$ crystals*, Physical Review Letters **60**, 2194 (1988).

[27] S. J. Larsson, *Resistivity in Cuprates and the Pseudogap*, Supercond Nov Magn **20**, 777 (2017).

[28] S. Naqib, J. Cooper, J. Tallon, and C. Panagopoulos, *Temperature dependence of electrical resistivity of high-T_c cuprates—from pseudogap to over-doped regions*, Physica C: Superconductivity **387**, 365 (2003).